Two-phase coexistence for hydrogen-helium mixtures

Riccardo Fantoni[*]

Dipartimento di Scienze Molecolari e Nanosistemi, Università Ca' Foscari Venezia, Calle Larga S. Marta DD2137, I-30123 Venezia, Italy

We use our quantum Gibbs ensemble Monte Carlo algorithm to perform computer experiments for the two-phase coexistence of a hydrogen-helium mixture. Our results are in quantitative agreement with the experimental results of Sneed, Streett, Sonntag, and Van Wylen. The difference between our results and the experimental ones is in all cases less than 15% relative to the experiment, reducing to less than 5% in the low helium concentration phase. At the gravitational inversion between the vapor and the liquid phase, at low temperatures and high pressures, the quantum effects become relevant. At extremely low temperature and pressure, the first component to show superfluidity is the helium in the vapor phase.

I. INTRODUCTION

Hydrogen and helium are the most abundant elements in the Universe. They are also the most simple. At ambient conditions, helium is an inert gas with a large band gap. Because of its low mass and weak interatomic interactions, it has fascinating properties at low temperatures, one of which is superfluidity. The molecular hydrogen and helium mixture is therefore of special theoretical importance since it is made by the two lightest elements in nature that have the lowest critical temperatures. This mixture is found to make up the atmosphere of giant planets such as Jupiter, and it is essential in stars.

An important problem to study is the phase coexistence of the fluid mixture and the determination of its coexistence properties. Some early experimental studies [1–3] have shown that at coexistence, at low temperature, the mixture shows a strong asymmetry in species concentrations in the liquid relative to the vapor phase, with an abundance of helium atoms in the vapor. This phenomenon results in the liquid floating above its vapor [3] since helium has approximately twice the molecular weight of hydrogen. Such experimental coexistence studies were later extended at higher temperature and pressure [4,5], allowing us to determine a quite complete picture for the coexistence phase diagram of this mixture in the temperature range from 15.5 to 360 K and in the pressure range from 5 bars to 75 kbars. Another interesting issue is whether this system exhibits fluid-fluid solubility at extremely high pressure [6–12], a situation that is hard to achieve in the laboratory.

In this work, we perform a numerical experiment for the two-phase coexistence problem of the hydrogen-helium mixture at low temperatures and pressures using the quantum Gibbs ensemble Monte Carlo (QGEMC) method recently devised [13,14] to solve the coexistence of a generic quantum boson fluid where the particles interact with a given effective pair potential. We will be concerned with situations in which the absolute temperature, T, and the number density, ρ_α, of each of the two components $\alpha = a,b$ of mass m_α are such that at least one of the two components is close to its degeneracy temperature $(T_D)_\alpha = \rho_\alpha^{2/3}\hbar^2/m_\alpha k_B$, with k_B the Boltzmann constant. For temperatures much higher than

$\max\{(T_D)_\alpha\}$, quantum statistics is not very important. This path-integral Monte Carlo simulation enables us to study the quantum fluid mixture from first principles, leaving the effective pair potentials between the two species, the hydrogen molecules, and the helium atoms as the only source of external information. There are studies on reproducing such coexistence from an equation-of-state approach [15]. Our QGEMC method is expected to break down at high densities near the solid phase. Moreover, clearly our approach becomes infeasible at extremely high pressures when the hydrogen is ionized, and one is left with delocalized metallic electrons [6–12].

Our binary mixture of particles of two species labeled by a Greek index, with coordinates $R \equiv \{\mathbf{r}_{i_\alpha} | i_\alpha = 1,2,\ldots,N_\alpha$ and $\alpha = a,b\}$ and interacting with a central effective pair-potential $\phi_{\alpha\beta}(r)$, has a Hamiltonian

$$\hat{H} = -\sum_{\alpha=1}^{2}\sum_{i_\alpha=1}^{N_\alpha} \lambda_\alpha \nabla_{i_\alpha}^2 + \frac{1}{2}\sum_{\alpha,\beta=1}^{2}\sum_{i_\alpha,j_\beta}' \phi_{\alpha\beta}(|\mathbf{r}_{i_\alpha} - \mathbf{r}_{j_\beta}|), \quad (1)$$

where the prime on the summation indicates that we must exclude the terms with $i_\alpha = j_\beta$ when $\alpha = \beta$ and $\lambda_\alpha = \hbar^2/2m_\alpha$.

The density matrix for the binary mixture at equilibrium at an absolute temperature T is then $\hat{\rho} = e^{-\beta\hat{H}}$ with $\beta = 1/k_B T$. Its coordinate representation $\rho(R,R',\beta)$ can be expressed as a path $[R(\tau)]$ integral in imaginary time (τ) extending from $R = R(0)$ to $R' = R(\beta)$ [16]. The many-particle path is made of $N = N_a + N_b$ single-particle world lines, which constitute the configuration space one needs to sample. Since the Hamiltonian is symmetric under exchange of like particles, we can project over the bosonic states by taking $\rho_B(R,R',\beta) = \sum_{\mathcal{P}} \rho(R,\mathcal{P}R',\beta)/(N_a!N_b!)$, where $\mathcal{P}$ indicates a permutation of particles of the same species.

If we call ρ the number density of the mixture, x_α the molar concentration of species α ($x_b = 1 - x_a$), $P = P(T,\rho,x_a)$ the mixture pressure, and $\mu_\alpha = \mu_\alpha(T,P,x_a)$ the chemical potential of species α, we want to solve the two-phase, I and II, coexistence problem,

$$\mu_a(T,P,x_a^{(\mathrm{I})}) = \mu_a(T,P,x_a^{(\mathrm{II})}), \quad (2)$$

$$\mu_b(T,P,x_a^{(\mathrm{I})}) = \mu_b(T,P,x_a^{(\mathrm{II})}) \quad (3)$$

_____

[*]rfantoni@ts.infn.it

TABLE I. Pair-potential parameters: ϕ_{pair}.

Pair	ε^*	r_m^*	α	β	γ	C_6	C_8	C_{10}	D
He-He	10.8	2.9673	13.208	13.353	0	1.3732	0.425 38	0.17810	1.2413
H$_2$-H$_2$	315 778	3.41	1.713	10.098	0.412 34	1.6955×10^{-4}	7.2379×10^{-5}	3.8984×10^{-5}	1.28
H$_2$-He	14.76	3.375	13.035	13.22	0	1.8310	0	0	0.798 02

for the concentrations $x_a^{(\text{I})}$ and $x_a^{(\text{II})}$ (and the densities $\rho^{(\text{I})}$ and $\rho^{(\text{II})}$) in the two phases. Since our mixture is not symmetric under exchange of the two species, a and b, we expect in general $x_a^{(\text{II})} \neq 1 - x_a^{(\text{I})}$.

Our QGEMC algorithm [14] uses two boxes maintained in thermal equilibrium at a temperature T and containing the two different phases. It employs a menu of seven different Monte Carlo moves: the *volume* move ($q = 1$) allows changes in the volumes of the two boxes assuring the equality of the pressures between the two phases, the *open-insert* ($q = 2$), *close-remove* ($q = 3$), and *advance-recede* ($q = 4$) allow the swap of a single-particle world line between the two boxes assuring the equality of the chemical potentials between the two phases, the *swap* ($q = 5$) allows us to sample the particle permutations, and the *wiggle* ($q = 6$) and *displace* ($q = 7$) allow us to sample the configuration space. We thus have a menu of seven, $q = 1, 2, \ldots, 7$, different Monte Carlo moves with a single random attempt of any one of them occurring with probability $G_q = g_q / \sum_{q=1}^{7} g_q$.

The paper is organized as follows: In Sec. II we describe the particular binary mixture studied, in Sec. III we describe the simulation method employed, in Sec. IV we present our numerical results, and Sec. V contains our final remarks.

II. THE H$_2$-He MIXTURE

We consider a binary fluid mixture of molecular hydrogen (H$_2$) and the isotope helium four (^{4}He), which are two bosons. We take 1 Å as the unit of length and k_B K as the unit of energy. An asterisk over a quantity indicates its reduced adimensional

value. We have the following for the parameter $\lambda_\alpha = \hbar^2/2m_\alpha$ of the two species $\alpha = \text{H}_2, {}^4\text{He}$:

$$\lambda_{\text{H}_2}^* = 12.032, \quad (4)$$

$$\lambda_{\text{He}}^* = 6.0596. \quad (5)$$

The pair-potential between two helium atoms is the Aziz *et al.* [17] HFDHE2, the one between two hydrogen molecules is that of Silvera *et al.* [18], and the one between a hydrogen molecule and a helium atom is that of Roberts [19,20]. All can be put in the following central form:

$$\phi(r) = \varepsilon \Phi(x), \quad (6)$$

$$\Phi(x) = \exp(\alpha - \beta x - \gamma x^2) - \left(\frac{C_6}{x^6} + \frac{C_8}{x^8} + \frac{C_{10}}{x^{10}} \right) F(x), \quad (7)$$

$$F(x) = \begin{cases} \exp[-(D/x - 1)^2], & x < D, \\ 1, & x \geqslant D, \end{cases} \quad (8)$$

where $x = r/r_m$, with r_m the position of the minimum, and the various parameters are given in Table I. We have $\phi_{\text{HeHe}}^*(r_m) = -10.8$, $\phi_{\text{H}_2\text{H}_2}^*(r_m) = -34.3$, and $\phi_{\text{H}_2\text{He}}^*(r_m) = -14.8$. Moreover, we have a slight positive nonadditivity: $[r_m^*]_{\text{H}_2\text{He}} = 3.375 > ([r_m^*]_{\text{HeHe}} + [r_m^*]_{\text{H}_2\text{H}_2})/2 = 3.189$.

The experimental coexistence data [1,3,4] are given in Table I of the Supplemental Material [21] and represented schematically in Fig. 1. For example, the mixture at $T = 31$ K has a lower critical state at $P = (0.207k_B)$ K Å^{-3}, $x_{\text{He}} = 0.214$ and an upper critical state at $P = (1.96k_B)$ K Å^{-3}, $x_{\text{He}} = 0.49$. The set of all critical states constitutes the x line, $T = T_x(P)$,
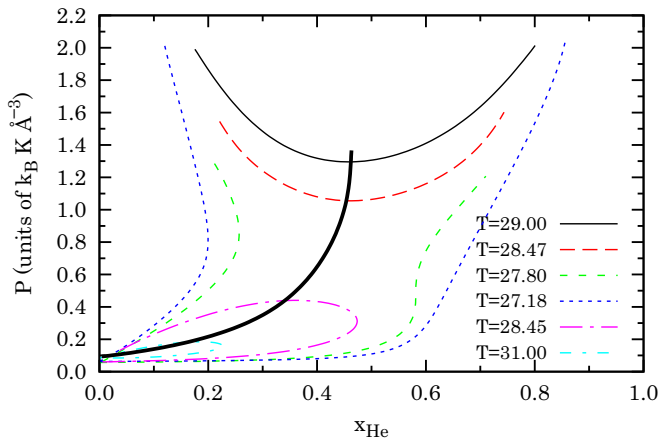

FIG. 1. (Color online) Schematic pressure-composition phase diagram for six isotherms of the hydrogen-helium mixture at low temperatures and low pressures as obtained in the experimental work by Streett *et al.* [4]. The thick continuous black line is the mixture critical line.
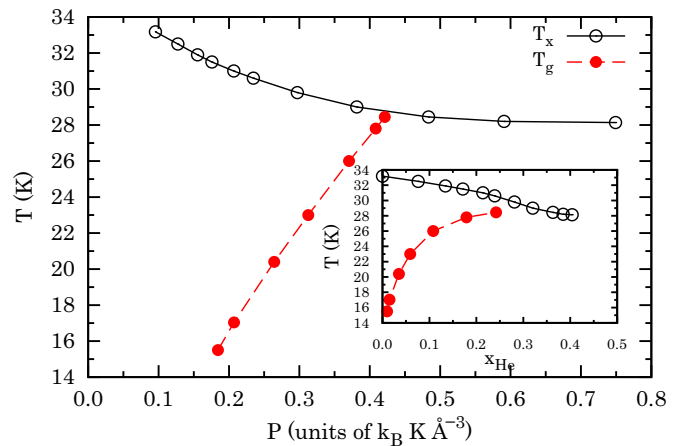

FIG. 2. (Color online) Reproduction of Fig. 3 of Sneed *et al.* [3] for the x line and the g line [see Eq. (11)]. The inset shows the two lines in the temperature-composition plane.

such that for $T > T_x$, then $x_{He}^{(I)} = x_{He}^{(II)}$. The experimental x line of Sneed *et al.* [3] is shown in Fig. 2 for the low-temperature and low-pressure mixture. In the figure, we also show the experimental line for the gravitational inversion described in Sec. III A.

For temperatures higher than the hydrogen critical point $T_{H_2} = 33.19$ K [$P_{H_2} = (0.094 k_B)$ K Å^{-3}] there is only an upper critical point [4]. At the temperature at which $T_x(P)$ reaches its minimum, there is no unanimous consensus among the various experimental works.

III. SIMULATION METHOD

We use our QGEMC method, described in Ref. [14], where we monitor the number densities of the two coexisting phases, $\rho^{(i)} = N^{(i)}/V^{(i)} = (N_{He}^{(i)} + N_{H_2}^{(i)})/V^{(i)}$ with $i = $ I,II, the concentrations of He in the two phases, $x_{He}^{(i)} = N_{He}^{(i)}/(N_{He}^{(i)} + N_{H_2}^{(i)}) < 1$, and the pressure P. We shall conventionally order $\rho^{(I)} < \rho^{(II)}$ so that I will be the vapor phase and II the liquid phase, unless $\rho^{(I)} = \rho^{(II)}$, in which case we have a fluid-fluid phase coexistence. In the simulation, we fix $N = N_{He}^{(I)} + N_{He}^{(II)} + N_{H_2}^{(I)} + N_{H_2}^{(II)}$ with $N_{H_2}^{(I)} + N_{H_2}^{(II)} = \chi[N_{He}^{(I)} + N_{He}^{(II)}]$ and $V = V^{(I)} + V^{(II)}$. Otherwise, $N_{He}^{(I)}, N_{He}^{(II)}, N_{H_2}^{(I)}, N_{H_2}^{(II)}$ and $V^{(I)}, V^{(II)}$ are allowed to fluctuate keeping $V^{(I)} + V^{(II)}$ and $N_{He}^{(I)} + N_{He}^{(II)}, N_{H_2}^{(I)} + N_{H_2}^{(II)}$ constants. The Gibbs phase rule for a two-phase coexistence of a binary mixture assures that one has two independent thermodynamic quantities [22]. So our control parameters will be the absolute temperature T and the global number density $\rho = N/V$ (instead of the pressure as in the experimental case). As usual, a finite N sets the size error for our calculation, whereas $\chi > 0$ will regulate the size asymmetry numerical effect, so that for

$$N_{He}^{(I)} = \frac{N x_{He}^{(I)}[1 - x_{He}^{(II)}(1+\chi)]}{(1+\chi)(x_{He}^{(I)} - x_{He}^{(II)})} > 0, \qquad (9)$$

$$N_{He}^{(II)} = \frac{N}{1+\chi} - N_{He}^{(I)} > 0, \qquad (10)$$

if $x_{He}^{(II)} < x_{He}^{(I)}$, we must have $0 < x_{He}^{(II)} < 1/(1+\chi) < x_{He}^{(I)} < 1$, and if $x_{He}^{(I)} < x_{He}^{(II)}$, then $0 < x_{He}^{(I)} < 1/(1+\chi) < x_{He}^{(II)} < 1$. Moreover, we must also always have $\rho^{(I)} < \rho < \rho^{(II)}$. The initial condition we chose for our simulations was always as follows: $\rho^{(I)} = \rho^{(II)} = \rho$ and $x_{He}^{(I)} = x_{He}^{(II)} = 1/(1+\chi)$.

Due to the short-range nature of the effective pair potentials of Eq. (6), we will approximate, during the simulation, $\phi(r) = 0$ for $r > r_{cut} \gg [r_m]_{H_2H_2}$ (this corresponds to the truncated *and* not shifted choice in Ref. [23]). To comply with the minimum image convention for the potential energy calculation, we make sure that the conditions $[V^{(i)}]^{1/3} > 2r_{cut}$ for $i = $ I,II are always satisfied during the simulation. This approximation is the only other source of error apart from the size error. The two are related because in the fluid-fluid coexistence, for instance, when $V^{(I)} \approx V^{(II)} \approx V/2$ during the simulation, we require $r_{cut} \approx (N/2\rho)^{1/3}/2 \gg [r_m]_{H_2H_2}$ for some given ρ.

The path-integral discretization imaginary time step $\delta\tau = \beta/K$, with K the number of time slices, is chosen so that

$\delta\tau^* = 0.002$, which is considered sufficiently small to justify the use of the primitive approximation of the interaction [16]. The parameters $\bar{M}$, defined in [14], will be called $\bar{M}_q$ for each relevant move q, and the parameter Δ_Ω, also defined in [14], is always chosen equal to 0.01. To fulfill detailed balance, we must choose $\bar{M}_2 = \bar{M}_3$. In particular, we always chose $\bar{M}_2 = 5$, $\bar{M}_3 = 5$, $\bar{M}_4 = 5$, $\bar{M}_5 = 5$, and $\bar{M}_6 = 5$. Regarding the frequency of each move attempt, we always chose $g_1 = 0.001$, $g_2 = 1$, $g_3 = 1$, $g_4 = 1$, $g_5 = 1$, $g_6 = 1$, and $g_7 = 0.1$. The parameter C defining the relative weight of the Z and G sectors [14] is adjusted, through short test runs, so as to have a Z-sector frequency as close as possible to 50%. We accumulate averages over 10^5 blocks each made of 10^5 attempted moves with quantities measured every 10^3 attempts. Since the volume move is the most computationally expensive one, we chose its frequency as the lowest. During the simulation, we monitored the acceptance ratios of each move. The various simulations took no more than $\sim$150 CPU hours on a 3 GHz processor.

A. Barotropic phenomenon and gravitational inversion

The condition for the gravitational inversion observed experimentally [3] is

$$\rho^{(I)}(m_{He}x_{He}^{(I)} + m_{H_2}x_{H_2}^{(I)}) > \rho^{(II)}(m_{He}x_{He}^{(II)} + m_{H_2}x_{H_2}^{(II)}), \quad (11)$$

where $m_{He}/m_{H_2} = 1.985\,53$. When this condition on the mass density inversion with respect to the number density is satisfied, the liquid phase will float on top of the vapor phase. The condition of Eq. (11) can also be rewritten as

$$\rho^{(I)}(1 + k x_{He}^{(I)}) > \rho^{(II)}(1 + k x_{He}^{(II)}), \qquad (12)$$

where $k = m_{He}/m_{H_2} - 1 = 0.985\,53$. This condition may be satisfied when the concentration of He in the vapor phase is bigger than that in the liquid phase at low temperatures, and the number density of the liquid is close to that of the vapor at high pressure. We expect quantum effects to become important in this regime before solidification, which is expected to occur for $T < T_s(P)$. The gravitational inversion of Eq. (12) will be satisfied for $T < T_g(P)$. The experimental s-line $T = T_s(P)$ and g-line $T = T_g(P)$ have been determined in Fig. 3 of Sneed *et al.* [3] in the laboratory.

B. Pressure calculation

We will use the virial estimator for the pressure [see Eq. (6.18) of Ref. [16]] with long-range corrections [24] that can be quite big in the liquid phase. More details on the pressure calculation are given in the Supplemental Material [21].

IV. NUMERICAL RESULTS

Our results are summarized in Table II and compared in Fig. 3 with the experimental data of Refs. [1,3,4] (summarized in a table in the Supplemental Material [21]).

In all of the studied cases, we chose $N = 128$ and $\delta\tau^* = 0.002$. We explored the vapor-liquid coexistence (in this work, we will denote as "vapor-liquid" coexistence the one in which $\rho^{(I)} \neq \rho^{(II)}$ at five temperatures, $T = 2, 5, 15.5, 26,$ and 31 K), and the fluid-fluid coexistence (we will denote as "fluid-fluid"
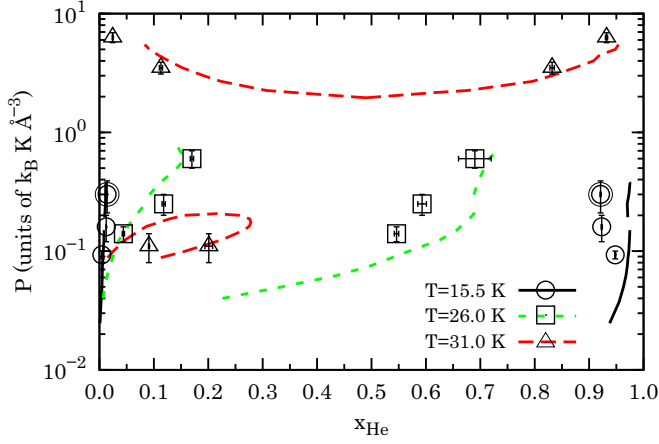
FIG. 3. (Color online) Comparison between the results of our numerical experiments (points from Table II) and of the laboratory experiments (lines from Table I in the Supplemental Material [21]) for the pressure-composition of three isotherms of the hydrogen-helium mixture phase diagram. A logarithmic scale is conveniently used on the ordinates. The double circled points at $T = 15.5$ K denote the case in which we observed gravity inversion in the numerical experiment.

coexistence the one in which $\rho^{(I)} = \rho^{(II)}$) at $T = 31$ K. For the first two lower temperatures studied, we could not find any experimental data for comparison. In these two cases, when we put a number with trailing dots in the table, it means that after the initial equilibration period, the measured property did not change anymore during the rest of the simulation.

For the temperature $T = 15.5$ K, as can be readily verified using the relation of Eq. (12), we observe gravitational inversion on the point at $\rho = 0.02$ Å^{-3} when the component with the highest degeneracy temperature is the hydrogen in the liquid phase with $T_D \approx 2$ K. Clearly when choosing higher pressures, quantum statistics will become more and more important for the fluid mixture before reaching the solid state.

For the points at $T = 26$ K, $T = 31$ K, $\rho = 0.006$ Å^{-3}, $\chi = 116/12$, $T = 31$ K, $\rho = 0.03$ Å^{-3}, and $\chi = 1$ we observed exchanges of identity between the two phases during the simulation.
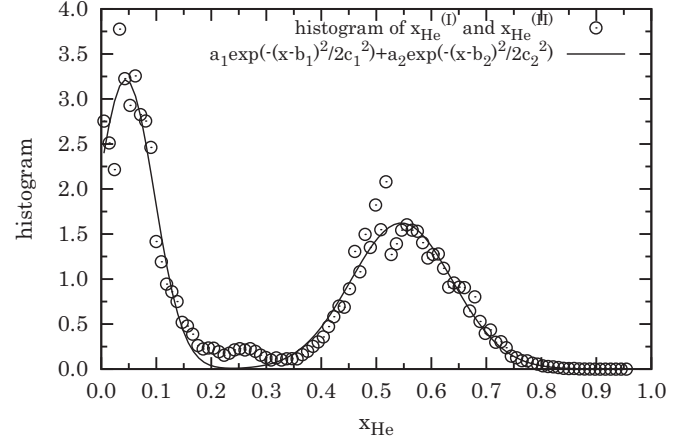

FIG. 4. Fit of the histogram for the block averages of both $x_{He}^{(I)}$ and $x_{He}^{(II)}$ with the sum of two Gaussians with six parameters. This is the case $T = 26$ K, $\rho = 0.01$ Å^{-3}, and $\chi = 90/38$, where we had box identity exchanges.

At a temperature $T = 31$ K and a pressure of $P = [0.07(2)k_B]$ K Å^{-3}, we found a vapor-liquid coexistence, choosing $\chi = 116/12$. This point should be subject to greater size error than all other points simulated, and thus should be less reliable, since we only have, in the two boxes, a total of 12 helium atoms. Increasing the pressure to $P = [0.21(2)k_B]$ K Å^{-3}, in agreement with the experiment, we did not find coexistence, and we observed $\rho^{(I)} \approx \rho^{(II)} \approx \rho$ and $x_{He}^{(I)} \approx x_{He}^{(II)} \approx 1/(1 + \chi)$. Increasing the pressure to $P = [3.5(4)k_B]$ K Å^{-3}, we did not observe exactly $\rho^{(I)} = \rho^{(II)}$, as measured in the fluid-fluid transition observed in the laboratory [4]. The same holds true for the point at the same temperature but higher pressure, $P = [6.3(6)k_B]$ K Å^{-3}.

For all measured points except the one at the lower temperature, $T = 2$ K of Table II, the superfluid fraction [25] of the two components in either phase was negligibly small. At $T = 2$ K of Table II, below the helium lambda-temperature, we observed a negligible superfluid fraction of both components in the liquid phase and of the hydrogen in the vapor phase.

TABLE II. Numerical isothermal pressure composition at coexistence. We always used $N = 128$ and $\delta\tau^* = 0.002$. All the pressures are in units of k_BKÅ^{-3}.

T (K)	ρ (Å^{-3})	χ	P	$x_{He}^{(II)}$	$x_{He}^{(I)}$	$\rho^{(II)}$ (Å^{-3})	$\rho^{(I)}$ (Å^{-3})
2.0	0.015	1	−0.08(7)	0.214...	0.639...	0.024 56(1)	0.012 605(2)
5.0	0.010	1	0.014(2)	0.1787(1)	1.000...	0.025 910(6)	0.005 113(1)
15.5	0.010	1	0.093(7)	0.00457(9)	0.948(1)	0.024 10(1)	0.006 544(5)
15.5	0.015	1	0.16(4)	0.0125(3)	0.923(1)	0.023 04(2)	0.011 525(7)
15.5	0.020	1	0.30(9)	0.0142(4)	0.921(1)	0.023 73(2)	0.017 619(5)
26.0	0.010	90/38	0.14(2)	0.044(2)	0.546(4)	0.018 90(5)	0.006 69(1)
26.0	0.015	90/38	0.25(5)	0.118(3)	0.593(8)	0.018 88(7)	0.011 05(5)
26.0	0.020	90/38	0.6(1)	0.170(3)	0.69(3)	0.021 15(2)	0.017 59(8)
31.0	0.006	116/12	0.11(3)	0.091(1)	0.201(7)	0.014(2)	0.005 64(6)
31.0	0.008	1	0.21(2)	0.5025(6)	0.511(1)	0.008 016(7)	0.007 95(1)
31.0	0.030	1	3.5(4)	0.832(4)	0.113(3)	0.031 98(4)	0.028 05(1)
31.0	0.035	1	6.3(6)	0.932(2)	0.0243(9)	0.039 55(5)	0.031 11(1)

TABLE III. Numerical isothermal pressure-composition coexistence at $T = 31$ K, $\rho = 0.03$ $\mathring{A}^{-3}$, and $\chi = 1$ as a function of the number of particles N. We always used $\delta\tau^* = 0.002$. All the pressures are in units of $k_B K \mathring{A}^{-3}$.

N	r_{cut} (Å)	P	$x_{He}^{(II)}$	$x_{He}^{(I)}$	$\rho^{(II)}$ ($\mathring{A}^{-3}$)	$\rho^{(I)}$ ($\mathring{A}^{-3}$)
64	5	2.4(8)	0.83(3)		0.03144(7)	0.02782(3)
128	6	3.5(4)	0.832(4)	0.113(3)	0.03198(4)	0.02805(1)
256	8	3.4(2)	0.840(3)	0.098(3)	0.03180(3)	0.028170(9)

The helium in the vapor phase was found to have a superfluid fraction of 0.012(3), indicating a tendency to superfluidity.

When we do not observe exchanges of identity between the two phases during the simulation, we are able to find accurate average values for the various measured quantities. Otherwise a histogram analysis of the data is necessary with a nonlinear fit using the superpositions of two shifted Gaussians. For example, in Fig. 4 we show the procedure used to extract the helium concentrations of the two coexisting phases for the case $T = 26$ K, $\rho = 0.01$ $\mathring{A}^{-3}$, and $\chi = 90/38$.

The measured property that is less accurate is the pressure due to the size error and the long-range correction dependent on the r_{cut} choice. This problem could be overcome by using the N,P,T version of the Gibbs ensemble algorithm instead of its N,V,T one [26].

A. Finite-size effects

We studied the finite-size effects at $T = 31$ K, $\rho = 0.03$ $\mathring{A}^{-3}$, and $\chi = 1$. In Table III, we show the results for the isothermal pressure-composition coexistence at $N = 64$, 128, and 256. As the number of particles increases, we observe a decrease in the ratio of the number of exchanges of identity between the two phases and the total number of particles: For $N = 64$, the exchanges occurred many times, for $N = 128$ only once, and for $N = 256$ never. For the case $N = 64$, we found the peak of the first Gaussian for the histogram of x_{He} with a negative value. The simulation with $N = 64$ took 1.0×10^5 s, the one with $N = 128$ took 1.6×10^5 s, and the one with $N = 256$ took 4.0×10^6 s. From the comparison we see that there is not much difference between $N = 128$ and 256. Apart from the smaller statistical errors in the latter case, the concentrations differ slightly in the two cases.

B. Importance of the particle exchanges and of the quantum effects

Setting to zero the frequency of the swap move attempts, our algorithm reduces to a path-integral calculation for distinguishable particles obeying the Boltzmann statistics. On the other hand, choosing $K = 2$ (with $\bar{M}_q = 1$ for all q) and $\lambda_{H_2}^* = \lambda_{He}^* \to 0$, our algorithm reduces to the classical Gibbs ensemble Monte Carlo (GEMC) algorithm of Panagiotopoulos [27].

For the state point $T = 15.5$ K and $\rho = 0.02$ $\mathring{A}^{-3}$ with $N = 128$, we performed two simulations for each of the two cases suggested above to estimate the importance of particle exchanges, which underlie the Bose-Einstein statistics, and of quantum effects, respectively. To reach the GEMC limit from our QGEMC algorithm, we chose, in particular, $\lambda_{H_2}^* = \lambda_{He}^* = 10^{-3}$. The results are shown in Table IV. The acceptance ratio for the swap move was around 0.5 in the full quantum case and imposed zero in the other two simulations.

As we can see from the table, for this state point, there is a very small difference between the path-integral simulation with the full Bose-Einstein statistics and the one with the Boltzmann statistics. In particular, only the densities of the vapor phase are different in the two cases. In both of these simulations, we observe the gravitational inversion. We expect that upon increasing the pressure and thereby the density or reducing the temperature, the particle exchanges will become increasingly important.

On the other hand, there is a large difference between these two simulations and the classical GEMC one. In particular, the gravitational inversion is not observed in the classical limit simulation, even if after a short equilibration time the simulation converged toward the condition $x_{He}^{(I)} = 1$, i.e., all helium atoms, the heaviest species in the mixture, were found in the less dense phase.

V. CONCLUSIONS

In conclusion, we performed path-integral Monte Carlo simulations using our QGEMC method for the two-phase coexistence of a hydrogen-helium mixture away from freezing. At low temperature, this asymmetric mixture displays a big concentration asymmetry in the two coexisting phases, whereas the densities of the two phases tend to become equal at high pressure. This is responsible for a gravitational inversion, where the liquid, the more dense phase, with an abundance of

TABLE IV. Numerical isothermal pressure-composition coexistence at $T = 15.5$ K, $\rho = 0.02$ $\mathring{A}^{-3}$, and $\chi = 1$ in a simulation with the full QGEMC algorithm with the Bose-Einstein statistics ($\delta\tau^* = 0.002$), with the QGEMC algorithm with Boltzmann statistics ($\delta\tau^* = 0.002$), and with the GEMC limit (see the main text) of the QGEMC algorithm. We always used $N = 128$. All the pressures are in units of $k_B K \mathring{A}^{-3}$.

Statistics	P	$x_{He}^{(II)}$	$x_{He}^{(I)}$	$\rho^{(II)}$ ($\mathring{A}^{-3}$)	$\rho^{(I)}$ ($\mathring{A}^{-3}$)
QGEMC: Bose-Einstein	0.30(9)	0.0142(4)	0.921(1)	0.02373(2)	0.017619(5)
QGEMC: Boltzmann	0.30(9)	0.0143(4)	0.919(1)	0.02373(2)	0.017638(5)
GEMC: classical limit	0.13(4)	0.000. . .	1.000. . .	0.035953(5)	0.0138552(7)

hydrogen, floats above the vapor, the less dense phase, with an abundance of helium. In this coexistence region of the temperature-pressure diagram, quantum statistics is expected to play an important role, and in our simulations we are able to observe such gravitational inversion. Our numerical experiments are also in good quantitative agreement with the experimental results of Sneed, Streett, Sonntag, and Van Wylen from the late 1960s and early 1970s. The difference between our results on the helium concentration in the two phases and the experimental ones is in all cases less than 15% in the high helium concentration phase and less than 5% in the low helium concentration phase, relative to the experiment.

These results for the hydrogen-helium mixture can be of interest for the study of cold exoplanets with an atmosphere composed predominantly of such a fluid mixture and with the right temperature and pressure conditions for there to be coexistence. In such cases, it could be possible to observe the gravitational inversion phenomenon and consequent changes in the planet moment of inertia, depending on the atmospheric and climatic conditions. At extremely low temperature and pressure, we find that the first component to show superfluidity is the helium in the vapor phase.

Our QGEMC method [14] is extremely simple to use, reduces to the Gibbs ensemble method of Panagiotopoulos [27] in the classical regime, and gives an exact numerical solution of the statistical physics phase coexistence problem for boson fluids.

An open problem currently under examination is the influence of the finite-size effects on the determination of the binodal curves close to the lower strongly asymmetric critical points, such as, for example, in our case $T = 31$ K, $\rho = 0.006$ Å^{-3}, and $\chi = 116/12$. This requires additional simulations at a higher and lower number of particles.

---

[1] W. B. Streett, R. E. Sonntag, and G. J. Van Wylen, J. Chem. Phys. **40**, 1390 (1964).

[2] R. E. Sonntag, G. J. Van Wylen, and R. W. Crain, Jr., J. Chem. Phys. **41**, 2399 (1964).

[3] C. M. Sneed, R. E. Sonntag, and G. J. Van Wylen, J. Chem. Phys. **49**, 2410 (1968).

[4] W. B. Streett, Astrophys. J. **186**, 1107 (1973).

[5] L. C. Van Den Bergh, J. A. Schouten, and N. J. Trappeniers, Physica A **141**, 524 (1987).

[6] B. Militzer, J. Low Temp. Phys. **139**, 739 (2005).

[7] M. A. Morales, E. Schwegler, D. Ceperley, C. Pierleoni, S. Hamel, and K. Caspersen, Proc. Natl. Acad. Sci. (USA) **106**, 1324 (2009).

[8] W. Lorenzen, B. Holst, and R. Redmer, Phys. Rev. Lett. **102**, 115701 (2009).

[9] W. Lorenzen, B. Holst, and R. Redmer, Phys. Rev. B **84**, 235109 (2011).

[10] J. M. McMahon, M. A. Morales, C. Pierleoni, and D. M. Ceperley, Rev. Mod. Phys. **84**, 1607 (2012).

[11] M. A. Morales, S Hamel, K. Caspersen, and E. Schwegler, Phys. Rev. B **87**, 174105 (2013).

[12] F. Soubiran, S. Mazevet, C. Winisdoerffer, and G. Chabrier, Phys. Rev. B **87**, 165114 (2013).

[13] R. Fantoni, Phys. Rev. E **90**, 020102(R) (2014).

[14] R. Fantoni and S. Moroni, J. Chem. Phys. **141**, 114110 (2014).

[15] Y. S. Wei and R. J. Sadus, Fluid Phase Equilibria **122**, 1 (1996).

[16] D. M. Ceperley, Rev. Mod. Phys. **67**, 279 (1995).

[17] R. A. Aziz, V. P. S. Nain, J. S. Carley, W. L. Taylor, and G. T. McConville, J. Chem. Phys. **70**, 4330 (1979).

[18] I. F. Silvera and V. V. Goldman, J. Chem. Phys. **69**, 4209 (1978).

[19] E. A. Mason and W. E. Rice, J. Chem. Phys. **22**, 522 (1954).

[20] C. S. Roberts, Phys. Rev. **131**, 203 (1963).

[21] See Supplemental Material at http://link.aps.org/supplemental/10.1103/PhysRevE.92.012133 for additional details on experimental data and calculations.

[22] L. D. Landau and E. M. Lifshitz, *Statistical Physics*, Pt. 1, 3rd ed., Course of Theoretical Physics (Butterworth Heinemann, Oxford, 1951), Sec. 86.

[23] B. Smit, J. Chem. Phys. **96**, 8639 (1992).

[24] M. P. Allen and D. J. Tildesley, *Computer Simulation of Liquids* (Clarendon, Oxford, 1987), Sec. 2.8.

[25] E. L. Pollock and D. M. Ceperley, Phys. Rev. B **36**, 8343 (1987).

[26] D. Frenkel and B. Smit, *Understanding Molecular Simulation* (Academic, San Diego, 1996), Chap. 8.

[27] A. Z. Panagiotopoulos, Mol. Phys. **61**, 813 (1987).